Basics of multiphoton effects in coherent radiation spectra

M V Bondarenco

NSC Kharkov Institute of Physics and Technology, 1 Academic St., 61108 Kharkov, Ukraine

E-mail: bon@kipt.kharkov.ua

Abstract. Differences between classically calculated radiation spectra of coherent radiation sources and their calorimetrically measured counterparts are discussed in a nutshell. Properties of photon multiplicity spectra are highlighted. The high-intensity limit is analyzed. A simple model for quick estimates of multiphoton effects in coherent radiation spectra is given.

1. Introduction

Ultra-relativistic character of radiation from high-energy electrons usually limits its experimental observation to angle-integral spectra, which are furthermore measured by electromagnetic calorimetry. But for intense gamma-radiation sources (e.g., coherent sources based on electron transmission through periodic structures), such spectra can significantly differ from classically evaluated ones (cf. Fig. 1), because an electron has a significant chance of emitting more than one photon, and only their total energy is measured by a calorimeter. Hence the need for establishing correspondence between single-photon spectra (photon number density) and multiphoton spectra (radiative energy loss probability distributions).

A detailed theory for multiphoton effects in coherent radiation spectra was offered in [1]. Here we present an outline of its results, along with some complementary remarks. In addition, we describe a crude model suitable for quickly obtaining expectations about coherent radiation spectrum shapes at a given intensity.

2. Generalities

If $\frac{dI}{d\omega_1}$ is a classically evaluated radiation energy spectrum, the rescaled distribution $\frac{dw_1}{d\omega_1} = \frac{1}{\omega_1}\frac{dI}{d\omega_1}$ can give the corresponding photon probability density only provided the integral

$$w_1 = \int_0^\infty d\omega_1 \frac{dw_1}{d\omega_1} \tag{1}$$

(the mean photon multiplicity) is small. Otherwise, $\frac{dw_1}{d\omega_1}$ can be used as a kernel for kinetic evolution of the distribution function for the radiating electrons,

$$\frac{\partial}{\partial L}\Pi(E_e-\omega) = \int_0^E d\omega_1 \frac{\partial}{\partial L}\frac{dw_1}{d\omega_1}\left[\Pi(E_e-\omega-\omega_1)-\Pi(E_e-\omega)\right], \qquad \Pi(E_e-\omega)\big|_{L=0} = \delta(\omega). \tag{2}$$

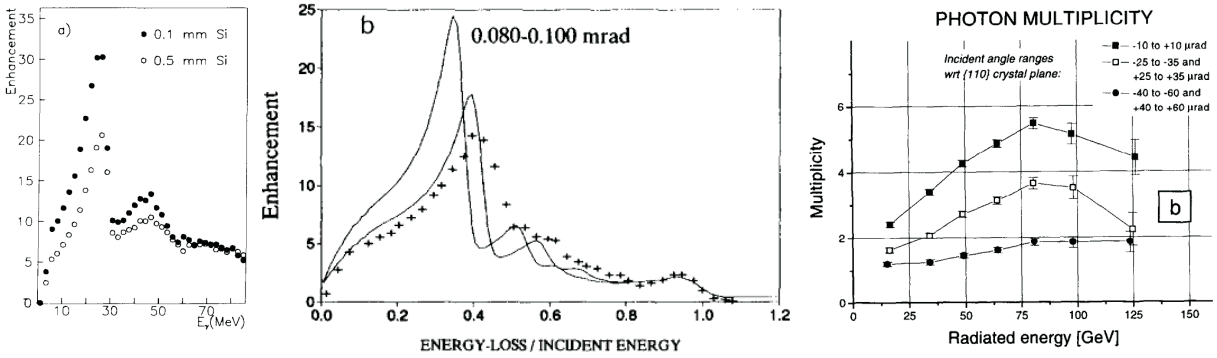

Figure 1. (a) Planar channeling radiation of 5 GeV positrons in (110) oriented Si crystal [2]. There is a difference between spectra (enhancement over the equivalent amorphous target) for crystal thickness $L = 0.1$ mm and $L = 0.5$ mm. (b) Coherent bremsstrahlung of 150 GeV electrons in a 0.6 mm thick (110) Si crystal. [3]. There is a difference between the calorimetrically measured (points) and the classically calculated radiation spectra (curves) [3]. (c) Photon multiplicities at coherent bremsstrahlung and planar channeling of 150 GeV electrons in 1.5 mm thick diamond crystal [4]. They exhibit a linear rise with ω, followed by a turnover.

or of the multiphoton spectrum,

$$\frac{\partial}{\partial L}\frac{dw}{d\omega} = \int_0^\infty d\omega_1 \left(\left.\frac{dw}{d\omega'}\right|_{\omega'=\omega-\omega_1} - \frac{dw}{d\omega} \right) \frac{\partial}{\partial L}\frac{dw_1}{d\omega_1} + W_0(L)\frac{\partial}{\partial L}\frac{dw_1}{d\omega}, \qquad \left.\frac{dw}{d\omega}\right|_{L=0} \equiv 0 \tag{3}$$

(inhomogeneous, but with a uniform initial condition). Quantities $\frac{dw}{d\omega}$ and Π are related via

$$\Pi(E_e-\omega) = \frac{dw}{d\omega} + W_0\delta(\omega), \qquad \int_0^{E_e} d\omega \Pi(E_e-\omega) = 1,$$

where $W_0 = 1 - \int_0^\infty d\omega \frac{dw}{d\omega} = e^{-w_1}$ is the photon non-emission probability.

The solution to the kinetic equation may be expressed as a contour integral in the complex s plane [1, 5]:

$$\frac{dw}{d\omega} = \frac{1}{2\pi i}\int_{c-i\infty}^{c+i\infty} ds e^{s\omega}\left[e^{\int_0^\infty d\omega_1 \frac{dw_1}{d\omega_1}(e^{-s\omega_1}-1)} - W_0 \right] \tag{4}$$

not involving probabilities differential in the traversed length L. The integral for $\Pi(E_e-\omega)$ is the same but without the W_0 term in the brackets. Another derivation of the contour integral representation for the resummed spectrum, not resorting to the notion of evolution with L, is based on the Poisson character of the soft photon emission process [6, 1].

Function $\Pi(E_e-\omega)$ has a δ-singularity at $\omega = 0$, whereas $dw/d\omega$ is regular everywhere. However, if integral (1) diverges on the lower limit, W_0 vanishes, and then $dw/d\omega = \Pi(E_e-\omega)$. That is the case for ionization losses, for which resummation of the type (4) was historically first carried out [5], but not always so for radiative energy losses [1].

Tips for numerical evaluation of the contour integral. At large $|\Im\mathrm{m}s|$, the integrand of (4) is oscillatory due to factor $e^{s\omega}$, with the oscillation amplitude decreasing insufficiently rapidly for direct numerical computation. To improve the convergence and facilitate the numerical evaluation, one may combine $e^{s\omega}$ with the differential, whereafter integrate by parts:

$$\frac{dw}{d\omega} = \frac{1}{2\pi i\omega}\int_{c-i\infty}^{c+i\infty} ds e^{s\omega + \int_0^\infty d\omega_1 \frac{dw_1}{d\omega_1}(e^{-s\omega_1}-1)} \int_0^\infty d\omega_1 \omega_1 \frac{dw_1}{d\omega_1} e^{-s\omega_1}. \tag{5}$$

If $\frac{dw_1}{d\omega_1} \underset{\omega_1\to 0}{\sim} \frac{a}{\omega_1}+b$, at large s we have $\int_0^\infty d\omega_1\omega_1\frac{dw_1}{d\omega_1}e^{-s\omega_1} \underset{s\to\infty}{\sim} \frac{a}{s}+\frac{b}{s^2}$, $\int_0^\infty d\omega_1\frac{dw_1}{d\omega_1}(e^{-s\omega_1}-1) \underset{s\to\infty}{\sim} -a\ln sE+\frac{b}{s}-\text{const}$, hence the integrand of (5) at $|\Im\mathrm{m}s|\to\infty$ decreases as s^{-1-a}. Such a rate of decrease may be sufficient, but still the integration must be carried out over a wide interval of s, and with a high working numerical precision, in order to account for significant cancellations with an oscillatory integrand. At small s, $\int_0^\infty d\omega_1\omega_1\frac{dw_1}{d\omega_1}e^{-s\omega_1} \underset{s\to 0}{\sim} \frac{a}{s}(1-e^{-sE})$, which has a cusp at $s\lesssim E^{-1}$. Therefore, in case of non-zero a, it may be sensible to choose constant $c>0$.

The role of averaging. The statistical independence of photon emissions holds only for a completely prescribed classical electromagnetic current. Therefore, any averaging procedures are to be performed *after* the resummation.

The integration over photon emission angles, though, may as well be performed before the resummation: if we do that after resummation, for angles of all the photons, we regain a resummation formula involving only the angle-integral single-photon spectrum.

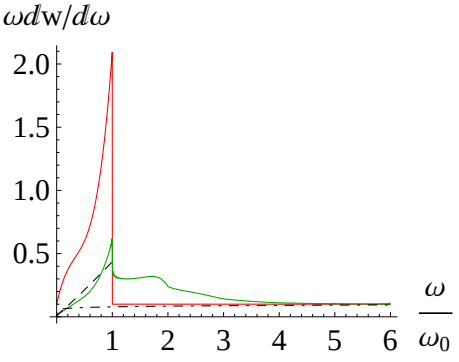

Figure 2. Red solid curve, single-photon spectrum of 'one-point' coherent bremsstrahlung, described by Eqs. (6-8), with parameters $E=10\omega_0$, $a=0.1$, $b\omega_0=\frac{3}{2}w_{1c}=2$ (moderate intensity). Green solid curve, the corresponding multiphoton spectrum. The second maximum originates entirely from multiphoton effects. Black dashed curve, low-ω asymptotics, $\omega\frac{dw}{d\omega}\simeq e^{-w_{1c}}\left(\frac{\omega}{E}\right)^a(a+b\omega)$. Black dot-dashed curve, high-ω asymptotics, $\omega\frac{dw}{d\omega}\simeq a\left(\frac{\omega}{E}\right)^a$.

3. Manifestation of multiphoton effects

In this section we will illustrate manifestation of multiphoton effects by a simple physical example. Adopt a 'one-point' dipole single-photon spectrum for the coherent radiation component:

$$\frac{dw_{1c}}{d\omega_1}=bP\left(\frac{\omega_1}{\omega_0}\right)\theta(\omega_0-\omega_1),\qquad P(z)=1-2z+2z^2, \tag{6}$$

with $\theta(z)$ the Heaviside unit step function, whereas the incoherent component is given by[1]

$$\frac{dw_{1i}}{d\omega_1}=\frac{a}{\omega_1}\theta(E-\omega_1), \tag{7}$$

and neglecting the interference, let

$$\frac{dw_1}{d\omega_1}=\frac{dw_{1c}}{d\omega_1}+\frac{dw_{1i}}{d\omega_1}. \tag{8}$$

An exemplary graph of the multiphoton spectrum corresponding to the single-photon spectrum (6) is shown in Fig. 2. We can see that multiphoton effects cause general lowering of the coherent radiation peak (like in Figs. 1a,b). Besides that, multiphoton effects alone can give rise to a second spectral maximum at $\omega\approx 2\omega_0$, and cause suppression at low ω, below the Bethe-Heitler value. A more detailed analysis is given in [1].

[1] Here the effective ultraviolet cutoff parameter E appears to differ from the electron energy E_e, and approximately equals $E\approx 0.5E_e$ (see [1, 6]).

High-intensity limit for pure coherent radiation. If coherent radiation intensity is high, but the incoherent radiation component is negligible, the contour integral (4) can approximately evaluated by the steepest descent method, yielding a Gaussian distribution:

$$\frac{dw_{\rm c}}{d\omega} \simeq \frac{1}{\sqrt{2\pi\overline{\omega_{1\rm c}^2}}} e^{-\rho^2/2} \qquad (w_{1\rm c} \gg 1). \tag{9}$$

Here $\rho = \frac{\omega - \overline{\omega_{1\rm c}}}{\sqrt{\overline{\omega_{1\rm c}^2}}}$ is the scaling variable, and $\overline{\omega_{1\rm c}} = \int_0^\infty d\omega_1 \omega_1 \frac{dw_{1\rm c}}{d\omega_1}$, $\overline{\omega_{1\rm c}^2} = \int_0^\infty d\omega_1 \omega_1^2 \frac{dw_{1\rm c}}{d\omega_1}$ are single-photon spectral moments.

It is interesting whether the Gaussian limit is achievable at practice. For that, besides high intensity, one also needs independence of the radiation spectrum on electron impact parameters, which are to be averaged over. In oriented crystals such a condition is nontrivial to fulfill. A possible case is radiation from electrons passing through a thick axially orientated crystal, wherein fair impact parameter independence may emerge due to the dynamical chaos and dechanneling. Fig. 3 shows the measured radiation spectrum under such conditions [7], along with a fit by formula (9). The fit may be regarded as acceptable, though not perfect. A better agreement can be obtained with the account of Chebyshev's correction for skewedness [1].

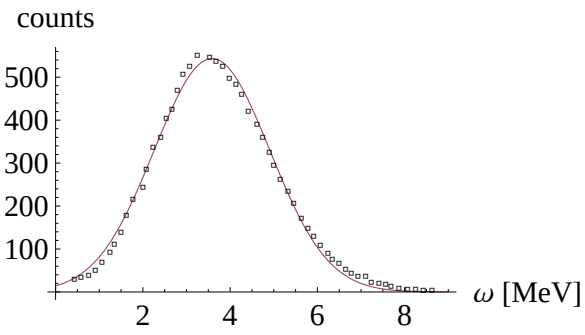

Figure 3. Energy loss probability spectrum for radiation from 40 GeV electrons traversing 2.5 cm thick Ge crystal along ⟨110⟩ axis. Points, experimental data [7]. Purple curve, the fit of Eq. (9) to the data.

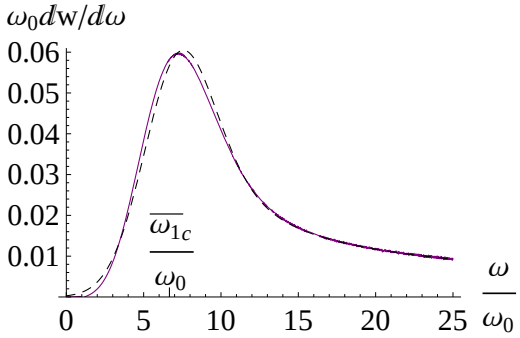

Figure 4. Multiphoton spectrum for single-photon spectrum (6-8) with parameters $b\omega_0 = 20$, $a = 0.3$. Solid purple curve, exact distribution; dashed black curve, parabolic cylinder approximation 10).

Impact of incoherent radiation on the high intensity limit. The incoherent bremsstrahlung component makes spectral moments diverge, thereby invalidating the Gaussian approximation. But still, the radiation in the Bethe-Heitler 'tail' is not intense enough for the Lévy asymptotics to become valid. Nonetheless, using convolution representations, we can attain an approximation suitable for $b\omega_0 \gg 1$, though $a < 1$ (intermediate between Gaussian and Lévy distributions) [1]:

$$\frac{dw}{d\omega} \approx \frac{1}{\sqrt{2\pi} E^a \overline{\omega_{1\rm c}^2}^{\frac{1-a}{2}}} e^{-\gamma_{\rm E} a - \rho^2/4} D_{-a}(-\rho), \tag{10}$$

$D_{-a}(z)$ being the parabolic cylinder function, and $\gamma_{\rm E} = 0.577$ Euler's constant. The behavior of distribution (10) is illustrated in Fig. 4.

4. Photon multiplicity spectrum

An observable complementary to the multiphoton spectrum is the photon multiplicity spectrum (for its definition and method of measurement see [1, 4]). For this observable, the resummation procedure gives [1]:

$$\bar{n}(\omega) = \frac{1}{dw/d\omega}\frac{1}{2\pi i}\int_{c-i\infty}^{c+i\infty} ds e^{s\omega+\int_0^\infty d\omega_1 \frac{dw_1}{d\omega_1}\left(e^{-s\omega_1}-1\right)} \int_0^\infty d\omega_1' \frac{dw_1}{d\omega_1'} e^{-s\omega_1'}. \tag{11}$$

Alternatively, the knowledge of $\frac{\partial}{\partial L}\frac{dw}{d\omega}$ from kinetic equation (3) or (2) may be used to obtain $\bar{n}(\omega)$ directly:

$$\bar{n}(\omega) = w_1 + L\frac{\partial}{\partial L}\ln\frac{dw}{d\omega}. \tag{12}$$

As an illustration, in Fig. 5 we show $\bar{n}(\omega)$ for the same conditions as in Fig. 2. There is a monotonous though stepwise rise in the region where the spectrum $\frac{dw}{d\omega}$ is well above the Bethe-Heitler value, and it changes into a falloff and a slow (logarithmic) increase where the Bethe-Heitler contribution dominates.

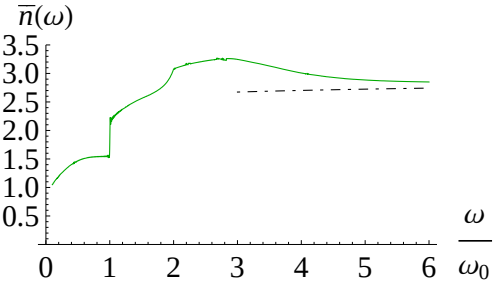

Figure 5. Solid green curve, photon multiplicity spectrum for the single-photon radiation spectrum given by Eqs. (6–8) with $a = 0.1$, $b\omega_0 = 2$, and $\epsilon = 0.1\omega_0$ (the infrared cutoff). Dot-dashed black curve, large-ω asymptotics $\bar{n}(\omega) \simeq w_{1c} + \bar{n}_i(\omega) = w_{1c} + 1 + a\ln\omega/\epsilon$.

At high radiation intensity, the Gaussian asymptotics of the spectrum $\frac{dw_c}{d\omega}$ corresponds to the linear asymptotics of the photon multiplicity spectrum:

$$\bar{n}_c(\omega) \approx w_{1c} + \frac{\overline{\omega_{1c}}}{\overline{\omega_{1c}^2}}\left(\omega - \overline{\omega_{1c}}\right) \qquad (w_{1c} \gg 1), \tag{13}$$

i. e., the step-like behavior smoothens out. Linear behavior (13) is in accord with the initial interval of experimental dependencies in Fig. 1c. With the account of incoherent radiation component, when $\frac{dw}{d\omega}$ obeys Eq. (10), $\bar{n}(\omega)$ expresses through parabolic cylinder functions, too (see [1]), and the initial linear dependence is followed by a turnover and subsequent logarithmic growth.

5. A toy model for coherent radiation

The generic features of multiphoton coherent radiation spectra may be elucidated by example of a simple model for the single photon spectrum[2]:

$$\frac{dw_1}{d\omega_1} = \frac{w_{1c}}{\omega_0}\theta(\omega_0 - \omega_1) + \frac{a}{\omega_1}\theta(E - \omega_1). \tag{14}$$

Inserting (14) to (4) gives the integral

$$\frac{dw}{d\omega} = e^{-w_{1c}-\gamma_E a}\frac{1}{2\pi i}\int_{c-i\infty}^{c+i\infty}\frac{ds}{(sE)^a}\exp\left[s\omega + \frac{w_{1c}}{\omega_0 s}\left(1 - e^{-s\omega_0}\right)\right]. \tag{15}$$

[2] The uniform spectral distribution of the coherent part (the first term) of $\frac{dw_1}{d\omega_1}$ corresponds to uniform angular distribution of radiation in electron rest frame, instead of $1 + \cos\tilde{\theta}^2$ typical for dipole radiation.

Expanding further $\exp[-\frac{w_{1c}}{\omega_0 s}e^{-s\omega_0}] = \sum_{n=0}^{\infty}\frac{1}{n!}\left(-\frac{w_{1c}}{\omega_0 s}\right)^n e^{-ns\omega_0}$ and integrating termwise, we get

$$\frac{dw}{d\omega} = \frac{e^{-w_{1c}-\gamma_E a}}{\omega_0}\left(\frac{\omega_0}{E}\right)^a \sum_{n=0}^{\lfloor\omega/\omega_0\rfloor}\frac{(-1)^n}{n!}w_{1c}^{\frac{n+1-a}{2}}\left(\frac{\omega}{\omega_0}-n\right)^{\frac{n-1+a}{2}} I_{n-1+a}\left\{2\sqrt{w_{1c}\left(\frac{\omega}{\omega_0}-n\right)}\right\}, \quad (16)$$

where I_{n-1+a} are the modified Bessel functions, and $\lfloor\omega/\omega_0\rfloor$ signifies the greatest integer smaller than ω/ω_0. Hence, for any given ω, the number of terms in the series is finite. Similarly, one can derive a closed formula for $\bar{n}(\omega)$, but it also involves derivatives of Bessel functions by index.

Eq. (16) can be used for quick generation of exemplary multiphoton distributions. Parameter w_{1c} is not in a strict correspondence with the magnitude of coherent radiation [say, b entering Eq. (6]. But since function P obeys inequality $\frac{1}{2} \le P(z) \le 1$ $(0 \le z \le 1)$, it seems reasonable to choose w_{1c} somewhere in the interval $\frac{1}{2}b\omega_0 < w_{1c} < b\omega_0$. In Fig. 6 we plot $\omega\frac{dw}{d\omega}$ for fixed a and several values of w_{1c}. The curve at moderate intensity (green band) can be compared with the green curve of Fig. 2. The correspondence is fair at $w_{1c} \approx \frac{4}{3} = \frac{2}{3}b\omega_0 = b\omega_0\int_0^1 dzP(z)$.

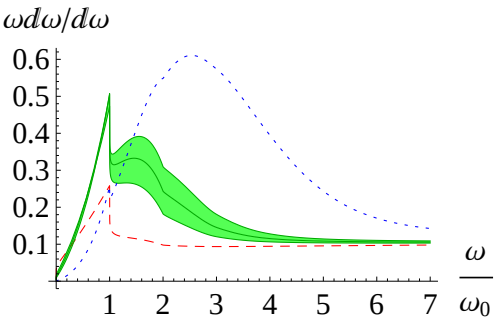

Figure 6. Energy spectra for coherent radiation described by formula (16), for parameters $E = 10\omega_0$, $a = 0.1$, and $w_{1c} = 0.3$ (red dashed curve); $\frac{4}{3} \pm \frac{1}{3}$ (green solid curves); 4 (blue dotted curve). The middle green curve is close in shape to the green curve of Fig. 2.

6. Concluding remarks

Multiphoton effects affect spectra of radiation in crystals with thicknesses $\gtrsim 1\%X_0$ (1 mm for Si). They not only bear on the overall normalization, but can also evoke a 2nd maximum, at $\omega \approx 2\omega_0$, similar to effect of secondary harmonics in the intra-crystal potential, or non-dipole effects. Besides that, they generate a suppression at low ω, superficially similar to LPM effect. Thus, one needs to be careful at interpretation of spectral features in medium-thickness crystals.

At implementation of the resummation procedure, it is essential that averaging over impact parameters must be performed at the final, not the initial stage. Sometimes that makes little difference, as for the case radiation in an amorphous medium; but it may be crucial in other cases, like for channeling radiation.

An inverse theoretical problem is the reconstruction of the single-photon spectrum from calorimetrically measured multiphoton one [8]. The complete reconstruction procedure for that (though restricted to conditions $\omega \ll E_e$ and the absence of strong averaging effects) was formulated in [1]. Its possible applications will be considered elsewhere.

References

[1] Bondarenco M V 2013 Multiphoton effects in coherent radiation spectra *Preprint* physics.acc-ph/1310.6681
[2] Bak J *et al.* 1985 *Nucl. Phys.* B **254** 491
[3] Medenwaldt R *et al.* 1991 *Phys. Lett.* B **260** 235
[4] Kirsebom K *et al.* 1996 *NIM* B **119** 79
[5] Landau L D 1944 *J. Phys. USSR* **8** 201
[6] Baier V N and Katkov V M 1999 *Phys. Rev.* D **59** 056003
[7] Medenwaldt R *et al.* 1989 *Phys. Lett.* B **227** 483
[8] Kolchuzhkin A, Potylitsyn A, Bogdanov A, and Tropin I 1999 *Phys. Lett.* A **264** 202; Kolchuzhkin A and Potylitsyn A 2001 *NIM* B **173** 126